iScience

CellPress
OPEN ACCESS

Article

Synthetic antibacterial discovery of symbah-1, a macrocyclic β-hairpin peptide antibiotic

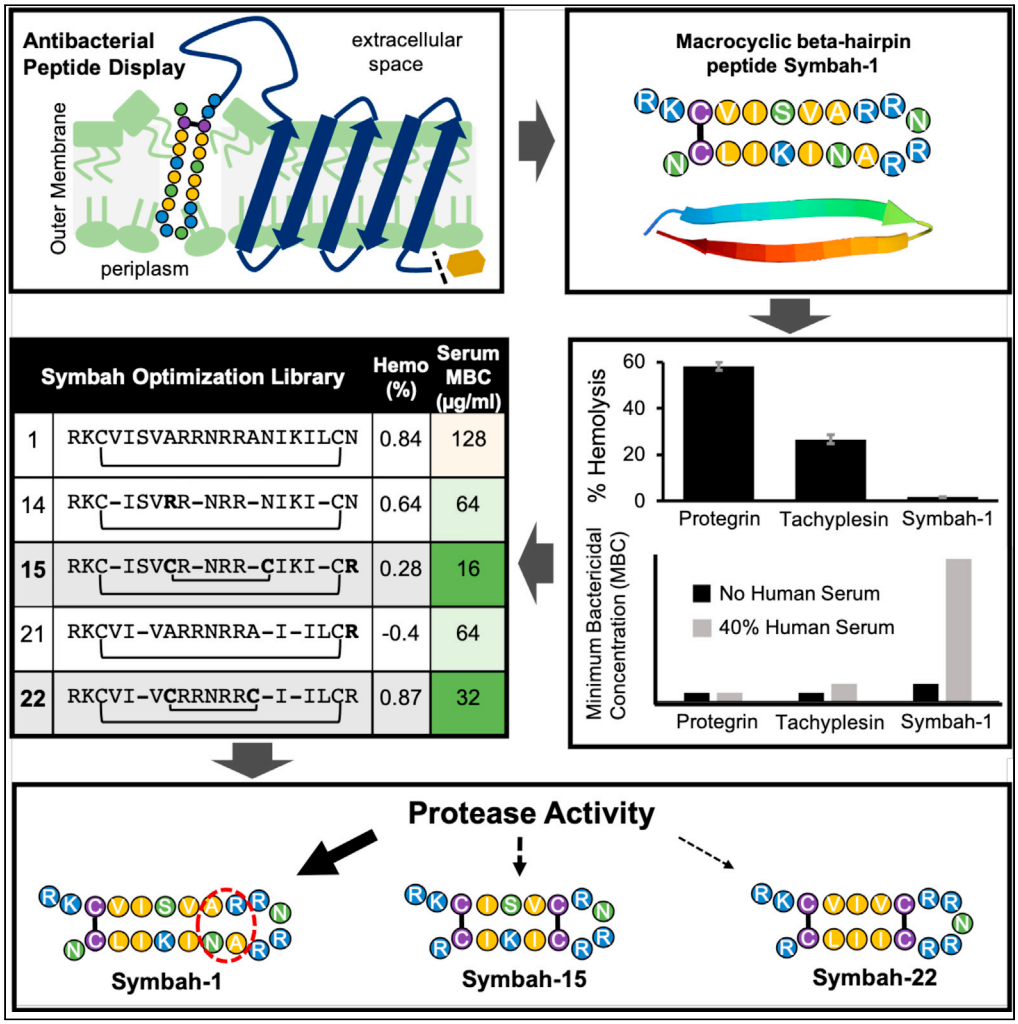

Justin R. Randall, Gillian Davidson, Renee M. Fleeman, ..., T. Jeffrey Cole, Cory D. DuPai, Bryan W. Davies

bwdavies@austin.utexas.edu

Highlights

Synthetic peptide display screen identifies a macrocyclic β-hairpin peptide antibiotic

Symbah-1 kills through disrupting bacterial membranes, yet is not very hemolytic

Symbah-1 loses activity in human serum, likely due to structural instability

Structural optimization improves its serum activity by reducing its protease lability

Randall et al., iScience 25, 103611
January 21, 2022
https://doi.org/10.1016/j.isci.2021.103611

iScience

CellPress
OPEN ACCESS

Article

Synthetic antibacterial discovery of symbah-1, a macrocyclic β-hairpin peptide antibiotic

Justin R. Randall,[1] Gillian Davidson,[1] Renee M. Fleeman,[1] Santos A. Acosta,[1] Ian M. Riddington,[2] T. Jeffrey Cole,[1] Cory D. DuPai,[1] and Bryan W. Davies[1,3,*]

SUMMARY

The rapid development and spread of antibiotic resistance necessitate the development of novel strategies for antibiotic discovery. Symbah-1, a synthetic peptide antibiotic, was identified in a high-throughput antibacterial screen of random peptide sequences. Symbah-1 functions through membrane disruption and contains broad spectrum bactericidal activity against several drug-resistant pathogens. Circular dichroism and high-resolution mass spectrometry indicate symbah-1 has a β-hairpin structure induced by lipopolysaccharide and is cyclized via an intramolecular disulfide bond. Together these data classify symbah-1 as an uncommon synthetic member of the β-hairpin antimicrobial peptide class. Symbah-1 displays low hemolysis but loses activity in human serum. Characterization of a symbah-1 peptide library identified two variants with increased serum activity and protease resistance. The method of discovery and subsequent characterization of symbah-1 suggests large synthetic peptide libraries bias toward macrocyclic β-hairpin structure could be designed and screened to rapidly expand and better understand this rare peptide antibiotic class.

INTRODUCTION

The rapid development of antibiotic resistance and the increased prevalence of multidrug-resistant (MDR) bacterial infections loom large over modern medicine (Centers for Disease Control and Prevention (U.S.), 2019; Shrivastava et al., 2018). Mining of culturable microbes, once a robust method of discovery, has stagnated; however, the decades long accumulation of active and inactive small- and macro-molecule datasets are beginning to allow advances in computational analysis and machine learning to rapidly screen for synthetic molecules with antibiotic (Randall and Davies, 2021).

Macrocyclic peptides have emerged as a promising avenue for the development of therapeutics (Passioura, 2020; Zorzi et al., 2017). Naturally occurring macrocyclic peptides have recently provided new antibiotic drugs, drug candidates, and scaffolds for development of novel antibiotics (Luther et al., 2018). Recently identified novel antibiotics such as teixobactin (Ling et al., 2015), lugdunin (Zipperer et al., 2016), darobactin (Imai et al., 2019), and murepavadin (Martin-Loeches et al., 2018) contain macrocyclic peptide-based structures. Several of these antibiotics, including teixobactin, darobactin, and murepavadin, function through the formation or mimicking of β-sheets to interact with their targets (Kaur et al., 2021; Zong et al., 2019). One rare class of potent peptide antibiotics are the β-hairpin antimicrobial peptides (β-AMPs). They contain an antiparallel β-hairpin structure and are cyclized via one or more intramolecular disulfide bonds (Panteleev et al., 2015, 2017). Members of this class can function through both membrane disruption and inhibition of essential proteins (Lam et al., 2006; Moura et al., 2020; Vetterli et al., 2018) and have served as scaffolds for therapeutic development (Edwards et al., 2017; Elliot et al., 2020; Orlov et al., 2019). Murepavadin, a synthetic derivative of the most well-studied β-AMP, protegrin-1, entered clinical development and specifically targets the *Pseudomonas aeruginosa* essential protein LptD (Andolina et al., 2018; Dale et al., 2018). Despite the promise of the β-AMP class, they remain understudied primarily due to their rarity and limited methods for new discovery.

Future development of peptide-based antibiotics hinges on overcoming issues of limited discovery, instability, and toxicity. Such limitations make strategies for high-throughput discovery and methods for improving stability while limiting toxicity essential. Recently, a high-throughput method of discovery called

[1]Department of Molecular Biosciences, University of Texas at Austin, Austin, TX 78712, USA

[2]Mass Spectrometry Facility, Department of Chemistry, University of Texas at Austin, Austin, TX 78712, USA

[3]Lead contact

*Correspondence: bwdavies@austin.utexas.edu

https://doi.org/10.1016/j.isci.2021.103611

surface localized antimicrobial display (SLAY) has demonstrated tremendous potential (Tucker et al., 2018). A screen of ~800,000 random peptides displayed on the surface of bacterial cells resulted in the identification of many novel sequences with antibacterial activity. Even with these additional means of discovery, peptide antibiotics still suffer from issues of instability, especially due to protease lability. There are several strategies for increasing their stability including constraining structure through cyclization (Moiola et al., 2019), altering the termini of peptides, and changing residues to nonnatural amino acids (Gentilucci et al., 2010). Such strategies tend to improve protease resistance, enhance serum activity, and in some cases reduce toxicity (Mourtada et al., 2019). Toxicity often occurs because antimicrobial peptides permeabilize mammalian membranes, but little is currently known about what characteristics impact β-AMP membrane selectivity. Changes in β-AMP conformation as well as differences in amphipathicity and hydrophobicity have been suggested, but a lack of unique sequences make analysis difficult (Edwards et al., 2016; Soundrarajan et al., 2019).

Here we characterize a synthetic macrocyclic β-hairpin antibiotic peptide (symbah-1) identified with SLAY. Symbah-1 is cyclized through an intramolecular disulfide bond and contains a β-hairpin structure induced by lipopolysaccharide (LPS). Symbah-1 has broad spectrum bactericidal activity and demonstrates *in vitro* and *in vivo* killing of carbapenem resistant *Acinetobacter baumannii*. It also exhibits a unique ability to differentiate between bacteria and erythrocyte membranes not common in natural members of the β-AMP class. Design and characterization of an optimization library identified several variants with increased serum activity and protease resistance. Symbah-1 represents the rare identification of a fully synthetic member of the β-AMP class, providing evidence that targeted SLAY screens could be used to rapidly increase β-AMP discovery and help elucidate sequence features affecting their stability, potency, and toxicity.

RESULTS

Symbah-1 is a peptide antibiotic functioning via membrane disruption

Symbah-1 was originally identified as a hit in an SLAY screen of random 20mer peptides performed in *Escherichia coli* W3110 (Tucker et al., 2018). This method involves screening large libraries of peptides for their ability to inhibit bacterial growth as a fusion protein tethered to the outer membrane (Figure 1A). Symbah-1 is cationic and has a sequence of RKCVISVARRNRRANIKILCNS containing two cysteines located toward its amino and carboxyl termini, potentially allowing cyclization via a disulfide bridge (Figure 1B). Induction of symbah-1 display on the surface of *E. coli* W3110 caused inhibition of growth in Luria-Bertani (LB) media when compared with no induction and induction of human influenza hemagglutinin (2xHA), a benign control (Figure 1C).

Because peptides are translated in linear form during SLAY screening, we chemically synthesized symbah-1 in linear form to begin testing *in vitro* activity. The minimum inhibitory concentration (MIC) of synthesized symbah-1 against *E. coli* W3110 was determined to be 16 μg/mL in Mueller-Hinton media (MH) and amidation of the carboxyl terminus improved the MIC to 8 μg/mL (Figure 1D). We went on to use amidated symbah-1 as the lead peptide for all subsequent experimentation. A killing curve was performed with symbah-1 at 2- and 4-fold its MIC in MH (Figure 1E). No colony-forming units (CFUs) were detected after 60 min of growth at either concentration. Because many bactericidal cationic antimicrobial peptides function through membrane disruption, we analyzed the ability of symbah-1 to permeabilize the *E. coli* W3110 inner and outer membranes through propidium iodide (PI) uptake (Figure 1F). PI is a fluorescent intercalating agent that binds DNA and can only access the cytoplasm if the inner and outer membrane have been permeabilized. *E. coli* W3110 cells were exposed to symbah-1 and 2xHA at 2- and 4-fold the MIC, and PI fluorescence was monitored. Treatment resulted in increased PI fluorescence with symbah-1, whereas there was no increase for treatment with 2xHA. Carbenicillin and polymyxin B were included as positive and negative controls respectively for this assay. These data suggest that symbah-1 is a bactericidal peptide antibiotic causing inner and outer membrane disruption.

Symbah-1 is a macrocyclic, β-hairpin peptide cyclized via a disulfide bond

We used a method incorporating machine learning called AlphaFold v2 to predict symbah-1 tertiary structure (Jumper et al., 2021). The primary model predicted a β-hairpin structure shared by a rare class of naturally occurring β-AMP antibiotics (Figure 2A). To analyze symbah-1 secondary structure we used circular dichroism spectroscopy (CD) with the addition of LPS. The structure of many peptide antibiotics is often induced by the presence of bacterial membranes or membrane mimics such as LPS (Avitabile et al., 2014). This includes β-AMPs such as protegrin-1, which demonstrate strong minima at 218 nm upon

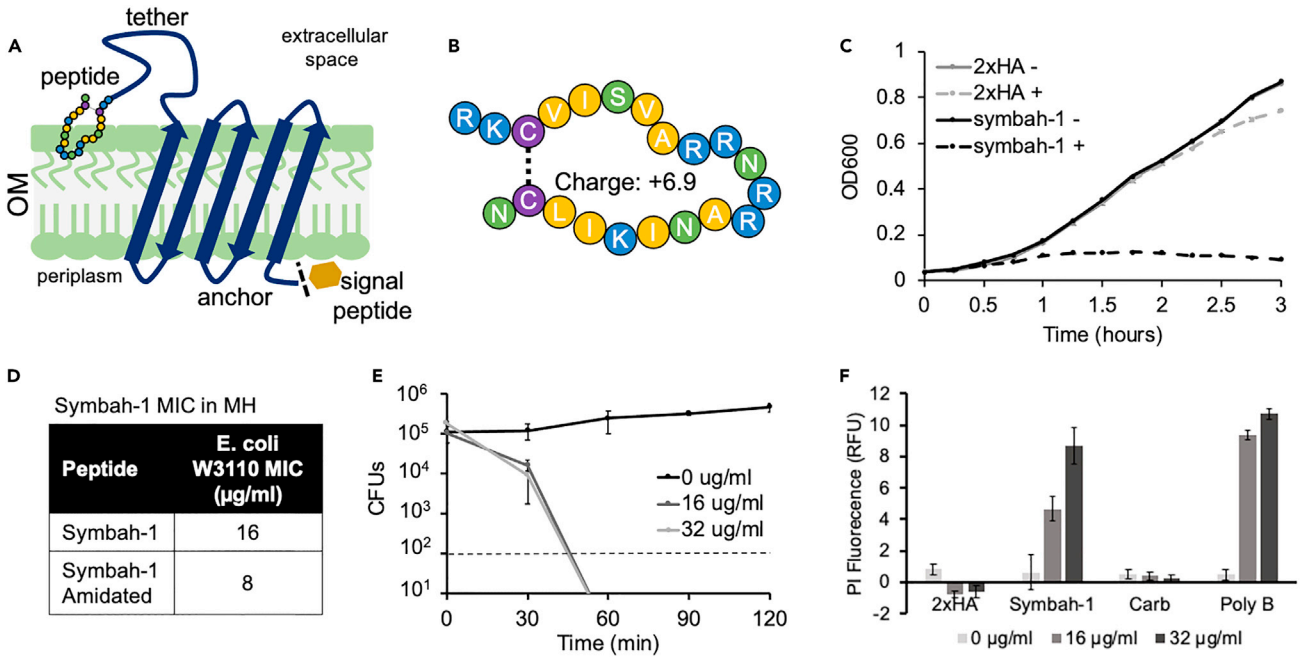

Figure 1. Symbah-1 is a peptide antibiotic functioning via membrane disruption

(A) Diagram of SLAY peptide display system in the outer membrane (OM).

(B) Symbah-1 peptide sequence (blue = charged, yellow = hydrophobic, green = polar, purple = cysteine).

(C) Growth curve with and without induction of peptide display (+/−). Data represented by mean +/- one standard deviation of triplicate samples (n = 3).

(D) Table showing *E. coli* W3110 MICs.

(E) Killing curve of *E. coli* W3110 cells treated with different concentration of symbah-1. Data are represented by the mean +/- one standard deviation of triplicate samples (n = 3). Error bars represent one standard deviation of triplicate samples (n = 3).

(F) PI uptake in relative fluorescence units (RFU) of *E. coli* W3110 cells challenged with different peptides and antibiotics. Data are represented by mean +/− one standard deviation of triplicate samples (n = 3).

addition of LPS (Soundrarajan et al., 2019). A CD spectrum with minimum at ~218 nm and maxima ~195 nm corresponds to an antiparallel β-sheet secondary structure (Greenfield and Fasman, 1969). CD spectra were determined for symbah-1 at varying concentrations of LPS (Figure 2B). Addition of LPS corresponds with a shift of minimum from ~200 nm (unstructured) to 218 nm (β-sheet), implying a likely antiparallel β-hairpin structure upon interaction with bacterial membranes.

Although symbah-1 was chemically synthesized in linear form, it contains two terminally localized cysteines that could create a disulfide bridge forming a macrocyclic peptide structure. To determine whether a disulfide bond spontaneously forms in symbah-1, we performed molecular weight analysis using high-resolution mass spectroscopy after suspension in MH. The presence of an intramolecular disulfide bond results in the loss of two hydrogen atoms corresponding to a drop of 2.016 daltons (Da) in the peptide's monoisotopic mass (M_{mi}). This shift in mass was confirmed by analyzing the mass-to-charge (m/z) ratio of the +5-charge state in MH of amidated symbah-1 chemically synthesized to contain a disulfide bond (cyclic) with and without addition of 10 mM dithiothreitol (DTT), a reducing agent that dissolves any disulfide bonds (Figure S1. High-resolution mass spectrometry of cyclized symbah-1 and Figure 2C). The isotope distributions for the +5-charge state of cyclic symbah-1 shifted with the addition of DTT corresponding to a ~2 Da increase in M_{mi} as expected. Our symbah-1 chemically synthesized without a disulfide bond matched the m/z isotope distribution and M_{mi} of cyclized symbah-1, suggesting it spontaneously forms a disulfide bond to form peptide macrocycle in MH media. Together our CD and MS data classify symbah-1 as a rare synthetic member of the small β-AMP class.

Macrocyclic structure is critical for activity due to decreased protease lability

To further examine symbah-1 function and the importance of cyclization, two cysteine to alanine symbah-1 variants (C3A and C20A) were chemically synthesized and compared with symbah-1 and chemically cyclized symbah-1. We first determined the MIC of each variant against *E. coli* W3110. Each variant lost ≥16-fold

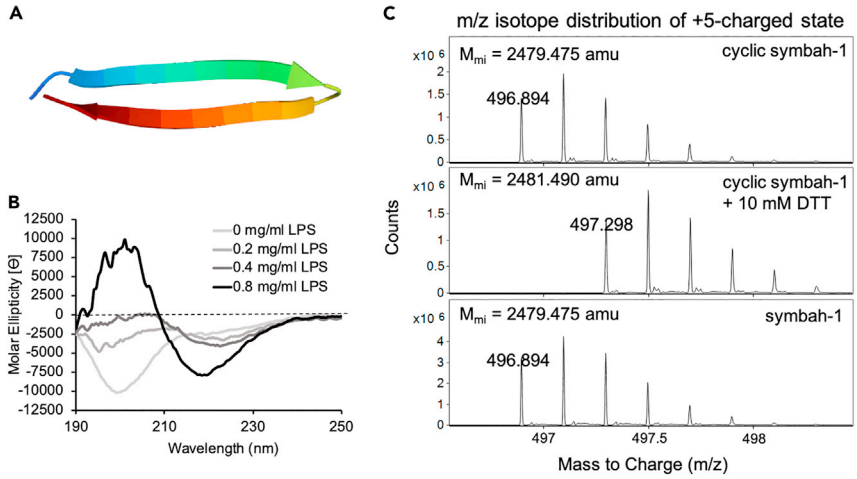

Figure 2. Symbah-1 is a synthetic member of the β-AMP class

(A) AlphaFold v2 model of symbah-1 tertiary structure.

(B) Circular dichroism spectra of symbah-1 with addition of various concentrations of LPS.

(C) High-resolution mass spectra of the +5 charge state isotope peaks of cyclic symbah-1 in MH, cyclic symbah-1 in MH + 10 mM DTT, and symbah-1 in MH. The measured M_{mi} (monoisotopic mass) of each peptide is inset top left.

activity relative to native symbah-1 (Figure 3A). We hypothesized that these variants may lose activity due to an inability to form a β-hairpin structure. To test this, CD spectra were examined for each variant and the cyclized version with LPS added (Figure 3B). A minimum was observed near 218 nm for each variant, suggesting each have the same relative β-hairpin structure even without the ability to cyclize. We next considered that an inability to cyclize may leave variants vulnerable to protease digestion. To explore this possibility minimum bactericidal concentrations (MBCs) were measured using an *E. coli* strain with cell envelope proteases deleted (HM130) and its parent strain (KS272) (Park et al., 1999). The MBC for KS272 was 8- to 16-fold higher for each cysteine variant relative to symbah-1, consistent with the previously observed increases in MIC for *E. coli* W3110. These differences were nearly eliminated when examining MBCs for the cell envelope protease knockout strain HM130 (Figure 3C). Addition of extracellular trypsin protease to the assay with HM130 increased the MBC for each cysteine variant while slightly reducing the MBC for symbah-1. These drastic changes in cysteine variant MBC with and without protease activity are likely due to increased protease lability because the MBC for symbah-1 and the chemically cyclized version of the peptide did not change more than 2-fold under each of the conditions tested. These data together suggest that the cysteine variants likely lose their activity due to increased protease lability when unable to form a disulfide bridge.

Symbah-1 has broad bactericidal activity against drug resistant pathogens

To investigate the spectrum of symbah-1 antimicrobial activity, MICs were determined for a panel of bacteria, including multiple pathogens from the antimicrobial-resistant ESKAPE group (*Enterococcus faecium*, *Staphylococcus aureus*, *Klebsiella pneumoniae*, *Acinetobacter baumannii*, *Pseudomonas aeruginosa*, and *Enterobacter* species). We measured MIC in both the canonical MH media and RPMI 1640 (RPMI), a media used for mammalian tissue culture. Symbah-1 inhibited the growth of each strain in both media (Figure 4A). Interestingly, the inhibitory activity ranged from 4 to 8 μg/mL in RPMI media for all the multidrug-resistant strains tested, including carbapenem-resistant *A. baumannii* (AB5075), carbapenemase-positive *K. pneumoniae* (ATCC 1705), and methicillin-resistant *S. aureus* (USA100) (Figure 4A). In addition, polymyxin-resistant strains, *E. coli* WD101 and *A. baumannii* R2, were similarly susceptible, as their parent strains *E. coli* W3110 and *A. baumannii* 17,978 suggesting symbah-1 may function differently from other cationic peptide antibiotics such as the polymixins (Figure 4A). The MIC of symbah-1 using RPMI was within 2-fold of several clinically used antibiotics against *A. baumannii* AB5075 (Figure 4B). *A. baumannii* AB5075 is a member of the carbapenem-resistant acinetobacter (CRA) group currently listed as an urgent threat by the CDC (Centers for Disease Control and Prevention (U.S.), 2019). To determine whether symbah-1 retains activity against *A. baumannii* AB5075 under *in vivo* conditions we ran a murine intraperitoneal infection model with and without injection of 5 mg/kg symbah-1 15 minutes after infection. Six hours postinfection the kidneys and liver of treated and

A Variant MIC in MH

Peptide	*E. coli* W3110 MIC (μg/ml)
symbah-1	8
C3A	128
C20A	128
cyclic symbah-1	16

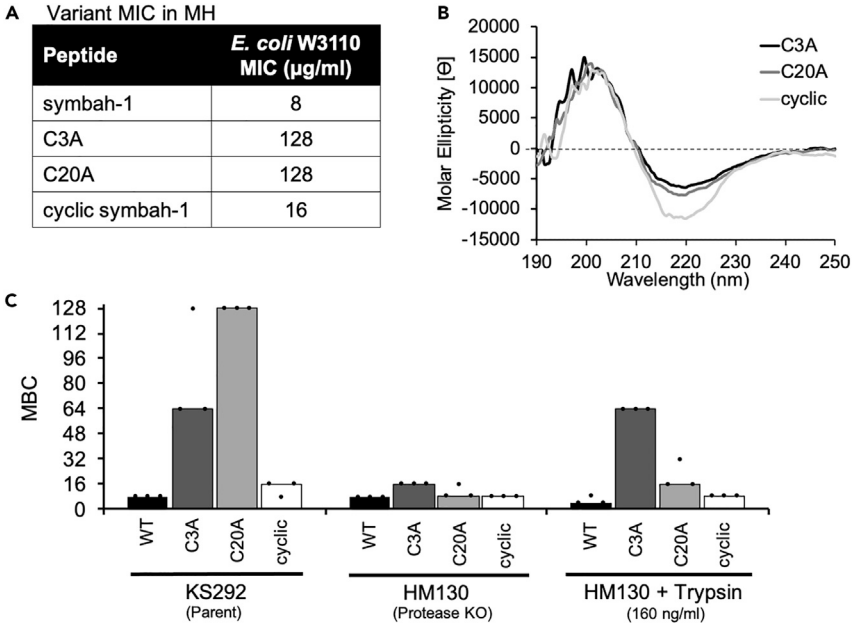

Figure 3. Macrocyclic structure is critical for activity due to reduced protease lability

(A) Symbah-1 variant peptide MICs against *E. coli* W3110.

(B) Circular dichroism spectra for symbah-1 variants with 0.8 mg/mL LPS.

(C) MBCs for symbah-1 variants against *E. coli* KS292, HM130, and HM130 with 160 ng/mL trypsin protease in MH media. Single dots represent individual replicates. Bars represent the median value (n = 3).

untreated mice were removed, homogenized, and plated for CFUs. A significant decrease in kidney and liver CFUs (p value <0.05) was observed for mice treated with symbah-1 relative to those without treatment, suggesting symbah-1 retains activity against *A. baumannii* AB5075 under *in vivo* conditions (Figure 4C). These data together suggest that symbah-1 has broad range activity on both gram-negative and gram-positive MDR bacterial pathogens and retains its activity under *in vivo* conditions.

Symbah-1 appears to have no strong secondary mechanism of action

Some β-AMPs such as thanatin have a mechanism of action targeting essential cell envelope processes (Fehlbaum et al., 1996; Moura et al., 2020; Vetterli et al., 2018). We thought it possible that symbah-1 may contain an additional mechanism of action, so we attempted to isolate *A. baumannii* AB5075-resistant mutants through subinhibitory serial passage in liquid media over two weeks. These attempts provided no isolates with improved resistance, suggesting resistance is not readily developed (Silver, 2011). Little is known about the genetic response of multidrug resistant strains challenged with membrane disrupting peptides so we examined the genetic response of *A. baumannii* AB5075 to symbah-1 treatment via RNA-seq to identify differentially regulated genes. We determined the $\log_2$-fold change in gene expression upon treatment with subinhibitory concentrations of symbah-1 (Table S1. AB5075 RNAseq and Table S2. Log_2-fold change in AB5075 gene expression). Interestingly, AB5075 upregulated two gene clusters and many genes of unknown function. A region from ABUW_1466 to ABUW_1471 was modestly upregulated. Many of these genes are homologous to general stress tolerance proteins such as LmbE. Another region from ABUW_2433 to ABUW_2443 was slightly more upregulated and includes many genes of unknown function. Three of these upregulated genes (ABUW_2443, _2679, and _2553) were not present in a transposon knockout library available from the University of Washington, suggesting they may be essential; however, ABUW_2443 and 2553 have extremely small open reading frames and may not been present due to low coverage. ABUW_2443 and ABUW_2679 have predicted Gram-negative sec secretion signals on their N-terminus, suggesting they may be present in the cell envelope where they would likely encounter symbah-1. Unfortunately, there was no clear effect on MIC when investigating any knockout or overexpression of all the upregulated genes tested (Table S1). We cannot rule out their involvement in combating symbah-1 activity because minor effects on cell death were not examined beyond minimum inhibitory concentration. Further investigation into some of these dysregulated genes may better elucidate their functions and possible involvement in response to

A Symbah-1 MICs against pathogenic bacteria

Bacterium	MIC in MH (μg/ml)	MIC in RPMI (μg/ml)
E. coli ATCC 25922	16	32
S. aureus USA100*	32	4
K. pneumoniae ATCC 1705*	32	8
A. baumannii AB5075*	16	4
P. aeruginosa ATCC 27853	32	8
E. hormaechei ATCC 49162	16	8
E. coli W3110	8	64
E. coli WD101†	16	64
A. baumannii 17978	16	4
A. baumannii R2†	16	8

* Denotes multidrug resistance
† Denotes polymyxin resistance

B Current AB5075 antibiotic MICs

	A. baumannii AB5075	
Antibiotic	MH MIC (μg/ml)	RPMI MIC (μg/ml)
Colistin	<0.25	2
Tigecycline	<0.25	2
Rifampin	0.5	4

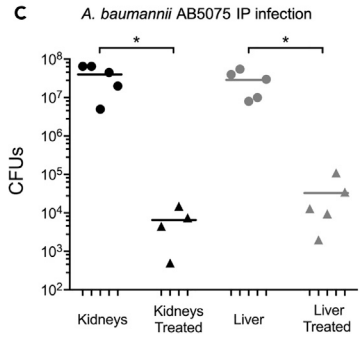

Figure 4. Symbah-1 has broad bactericidal activity against drug resistant pathogens

(A) Table of symbah-1 MICs against various bacterial strains in MH media and RPMI media.

(B) Table of clinically relevant antibiotics against *A. baumannii* AB5075 in MH media and RPMI media.

(C) CFUs of the kidneys and liver resulting from injection of 1×10^6 *A. baumannii* AB5075 cells in the mouse intraperitoneal space with and without treatment with 5 mg/kg symbah-1. Filled circles or triangles represent CFUs from a single replicate; lines represent the mean of all replicates from one condition (* two-tailed t test p value ≤ 0.05) ($n \geq 4$).

symbah-1 membrane disruption. Lastly, we performed a pull-down on a 6× histidine tagged version of symbah-1 retaining antibacterial activity in an attempt to identify potential protein interactors. A comparison of mass spectrometry analysis from pull-downs of 6× histidine tagged symbah-1 and tagless symbah-1 following treatment of *A. baumannii* 17,978 cells revealed no obvious, significant protein interactors (Table S3. Symbah-1 pull down). These data together suggest that symbah-1 membrane disruption is most likely the primary mechanism of killing and that resistance to symbah-1 activity is not readily developed.

Symbah-1 has low hemolysis but loses activity in human serum

Antimicrobial peptides used therapeutically have to overcome issues of toxicity and serum stability in order to successfully treat disease. For this reason, we decided to compare the hemolysis and serum activity for symbah-1 and the sequences of two naturally occurring membrane disrupting β-AMPs, protegrin-1 (Kokryakov et al., 1993) and tachyplesin-1 (Nakamura et al., 1988). We had their peptide sequences chemically synthesized and verified their β-hairpin structure via CD with LPS and membrane activity via PI uptake (Figure S2. Protegrin-1 and tachyplesin-1 function and structure). The hemolysis of 2-fold serially diluted protegrin-1 and tachyplesin-1 were determined and compared with hemolysis observed with 1% Triton X-100 (100%). Thanatin, a β-AMP previously reported to have very low hemolysis (Edwards et al., 2016), was used as a negative control. Interestingly, symbah-1 showed very low hemolysis relative to protegrin-1 and tachyplesin-1 (Figure 5A), suggesting symbah-1 may have unique membrane selectivity in comparison to membrane disrupting members of the natural β-AMP class. Next, MBCs were determined with and without the presence of 40% human serum for each peptide in MH. MBCs were used because the addition of serum affected the optical density used to determine MIC. The MBCs of all three β-AMPs were within 2-fold of one another ranging from 8 to 16 μg/mL; however, symbah-1 lost 8-fold activity when 40% human serum was added, whereas protegrin-1 and tachyplesin-1 had no change and a 2-fold change, respectively (Figure 5B). We decided to examine the number of disulfide bonds present in each peptide resuspended in PBS using liquid chromatography paired with mass spectrometry (LC/MS) to predict their conformation more accurately under *in vivo* conditions (Figure 5C). Protegrin-1 and tachyplesin-1 eluted off the liquid chromatography column as a single peak and contained two disulfide bonds, as their measured monoisotopic masses were ~4 Da lighter than the expected M_{mi} with no disulfide bonds present (Figure 5C). Interestingly, symbah-1 eluted as two distinct peaks. Mass spectrometric analysis of each individual peak showed one contained a disulfide bond and the other did not (Figure S3. Calculating peptide percent cyclization). The peak containing a disulfide bond represented 43% ± 1 of the area of all peaks. This suggests that symbah-1 exists in both cyclized and linear conformations in PBS in contrast to MH media. The number and percentage of disulfide bonds present in

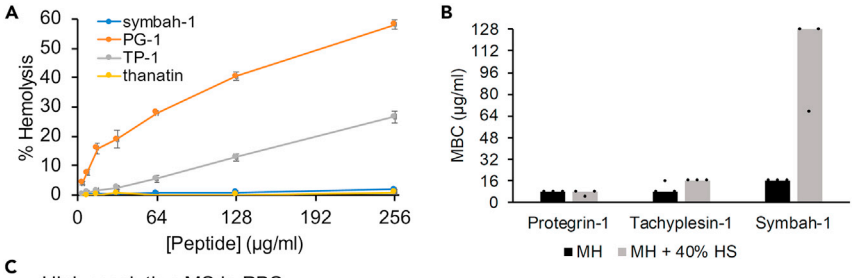

C

High resolution MS in PBS.

Peptide	Measured M_{mi} (Da)	Expected Linear M_{mi} (Da)	ΔM_{mi} (Da)	# S-S bonds	Percentage (%)
protegin-1	2155.080	2159.060	3.980	2	100 ± 0
tachyplesin-1	2263.100	2267.085	3.985	2	100 ± 0
symbah-1	2479.475 2481.490	2481.438 -	1.963 -0.052	1 0	43 ± 1 57 ± 1

Figure 5. Symbah-1 has low hemolysis but loses activity in human serum

(A) Percent hemolysis of serial dilutions of symbah-1, protegrin-1 (PG-1), tachyplesin-1 (TP-1), and thanatin. Error bars represent one standard deviation (n = 3).

(B) MBCs of β-AMPs with MH and MH with 40% human serum (HS). Single dots represent single replicates of triplicate experiments. Bars represent the median value.

(C) Table of M_{mi} (monoisotopic mass) for β-AMPs in PBS as determined by high-resolution LC/MS. Data are represented by mean +/− one standard deviation of triplicate samples (n = 3).

protegrin-1, tachyplesin-1, and symbah-1 in PBS could help explain the differences observed in their serum activities.

Design of a symbah-1 optimization library

To help determine why symbah-1 loses significant activity in human serum we designed a variant library attempting to increase its stability. Protegrin-1 and tachyplesin-1 have tightly constricted β-hairpin structures involving two disulfide bonds (Figure S4. Beta-hairpin antimicrobial peptide structures). Symbah-1 is slightly longer, has only one potential disulfide bond, and may have a strained loop region due to incompatible R-group pairs near the turn of its β-hairpin structure (Figure S4). To remedy these potential issues and inform our library design we first determined the importance of each residue in the symbah-1 sequence by measuring the MIC against *A. baumannii* AB5075 with crude alanine variants at each position in both MH and RPMI media (Figure S5. Symbah-1 residue importance). Using this information, we then generated an unamidated symbah-1 optimization library (SBH), trying to alter only flexible residues and increase structural stability through a combination of matching potential antiparallel β-sheet R-group pairs and adding the potential for an additional disulfide bond (Table 1). We also made attempts to retain both the charge and β-hairpin structure of symbah-1 in the SBH library. After the initial library design, we predicted the tertiary structure of all 24 designed peptides in the library using AlphaFold2 modeling (Figure S6. AlphaFold tertiary structure modeling). The primary model for each SBH peptide was predicted to have a β-hairpin structure apart from SBH-16 whose secondary model was a β-hairpin. We went ahead and had all 24 SBH peptides chemically synthesized for further characterization.

Symbah-1 variants contain increased serum activity and low hemolysis

To evaluate our designed library, the secondary structure, disulfide bond state, serum activity, and hemolysis were determined for each SBH peptide. Only a ≥ 4-fold improvement of antibacterial activity over SBH-1 was considered significant due to differences in peptide purity (see Table S5. Peptides used). One peptide, SBH-19, was insoluble in water and was therefore removed from the library.

First, the β-hairpin structure of each peptide in the library was confirmed using CD with addition of 0.8 mg/mL LPS (Figure S7. SBH peptide circular dichroism). All peptides appeared to retain β-hairpin structure with LPS present, although minor increases in minima wavelength were observed. Next, the number and percentage of

Table 1. Characterization of a symbah-1 optimization library

Name	Sequence	Hemo (%)	MH MBC (μg/mL)	MH + HS MBC (μg/mL)	RPMI MBC (μg/mL)	RPMI + HS MBC (μg/mL)	Single S-S (%)	Two S-S (%)	GRAVY
SBH-1	RKCVISVARRNRRANIKILCN-	0.84	32	>128	8	>128	29	–	−0.348
SBH-2	RKCVISVARRNRRANI**Y**ILC**R**-	2.02	64	>128	2	128	38	–	−0.271
SBH-3	RKCVI**L**VARRNRRANI**V**ILC**R**-	4.23	32	128	4	128	50	–	0.210
SBH-4	RKCVISVARRNRR**NA**IKILCN-	0.40	32	128	8	128	33	–	−0.348
SBH-5	RKCVI**L**VARRNRR**NA**I**V**ILC**R**-	7.52	64	128	2	128	34	–	0.210
SBH-6	RKCVIS**C**ARRNRRAN**C**KILCN-	−0.15	32	>128	16	>128	48	52	−0.524
SBH-7	RKCVIS**C**ARRNRR**NAC**KILCN-	−0.21	32	128	16	>128	19	63	−0.524
SBH-8	RKCVI**LC**ARRNRR**NACV**ILC**R**-	6.52	32	64	2	32	12	33	0.033
SBH-9	RKCVISV**RI**RNRRANIKILCN-	0.18	32	128	4	128	39	–	−0.219
SBH-10	RKC**Q**ISV**RI**RNRRANIKI**S**CN-	−0.11	>128	>128	128	>128	66	–	−0.805
SBH-11	RKC**Q**ISC**RI**RNRRANC**K**I**S**CN-	1.60	32	64	8	64	8	46	−0.981
SBH-12	RKCVISC**RI**RNRRANCKILCN-	0.62	32	128	4	64	2	51	−0.395
SBH-13	RKC-ISV**RI**RNRRANIKI-CN-	0.08	32	128	16	>128	98	–	−0.663
SBH-14	RKC-ISV**R**R-NRR-NIKI-CN-	0.64	128	>128	>128	>128	98	–	−1.112
SBH-15	RKC-ISV**C**R-NRR-**C**IKI-C**R**-	0.28	8	16	8	16	24	37	−0.406
SBH-16	RKCVISVARRNRRA-IKILCN-	−0.03	32	>128	8	>128	88	–	−0.190
SBH-17	RKCVISV**C**RRNRR**C**-IKILCN-	1.13	64	64	16	64	59	41	−0.120
SBH-18	RKCVI**L**VARRNRRA-I**V**ILC**R**-	3.46	32	128	4	>128	43	–	0.395
SBH-20	RKCVI**LC**AR-NRRA-**CV**ILC**R**-	3.54	32	64	4	128	0	74	0.458
SBH-21	RKCVI-VARRNRRA-I-ILC**R**-	−0.40	8	128	2	128	59	–	−0.006
SBH-22	RKCVI-V**C**RRNRR**C**-I-ILCR-	0.87	16	32	4	32	8	92	0.072
SBH-23	RKCVI-VAR-NRRA-I-ILC**R**-	−0.13	8	>128	8	>128	100	–	0.259
SBH-24	RKCVI-V**C**R-NRR**C**-I-ILC**R**-	3.79	32	64	8	128	0	100	0.341
SBH-15[a]	RKC-ISV**C**R-NRR-**C**IKI-C**R**-	–	8	16	8	16	–	–	–

Hemo, hemolysis; MH, Mueller-Hinton; HS, 40% human Serum; S-S, disulfide bond.
[a]C-terminal amidation; GRAVY, grand average of hydropathicity index; Bold, residue change.

disulfide bonds present in PBS for each peptide were evaluated using LC/MS. Like symbah-1, most SBH peptides presented a mixture of conformations in PBS, which were separated during the liquid chromatography phase of the assay. The number of disulfide bonds present for each LC peak were determined by M_{mi}, and percentages were calculated for each based on the relative area of each liquid chromatography peak (see Figure S3. Calculating peptide percent cyclization and Table 1). The addition of a second cysteine pair to SBH peptides resulted in a proportion with two disulfide bonds present. These percentages varied, suggesting each peptide's ability to spontaneously form either one or two disulfide bonds may be impacted by structural changes determined by sequence variation.

Next, the serum activity for each peptide in the library was measured by comparing MBCs against *A. baumannii* AB5075 in MH and RPMI with and without 40% human serum. SBH-1 lost activity in 40% human serum in both media similar to what was observed with symbah-1. There was a strong correlation between peptides with some proportion containing two disulfide bonds and retained serum activity. Although, this correlation was not due to an additional disulfide alone (Table 1, SBH-6). The two peptides with the greatest retention of serum activity were SBH-15 and SBH-22, gaining ≥ 8-fold activity in serum relative to SBH-1 in both media.

Lastly, the hemolysis of each SBH peptide was also determined at 128 μg/mL (Figure S8 and Table 1). We observed that all SBH peptides still contained relatively low hemolysis compared with protegrin-1 and tachyplesin-1; however, there seemed to be a correlation between replacement of the S6/K17 pairing and increased percent hemolysis. These changes could be explained by the corresponding increase in GRAVY score, a measurement of overall peptide hydrophobicity, although there were exceptions (SBH-22 and SBH-23). SBH-15 and SBH-22 stood out as the two peptides with the greatest improvement in serum activity

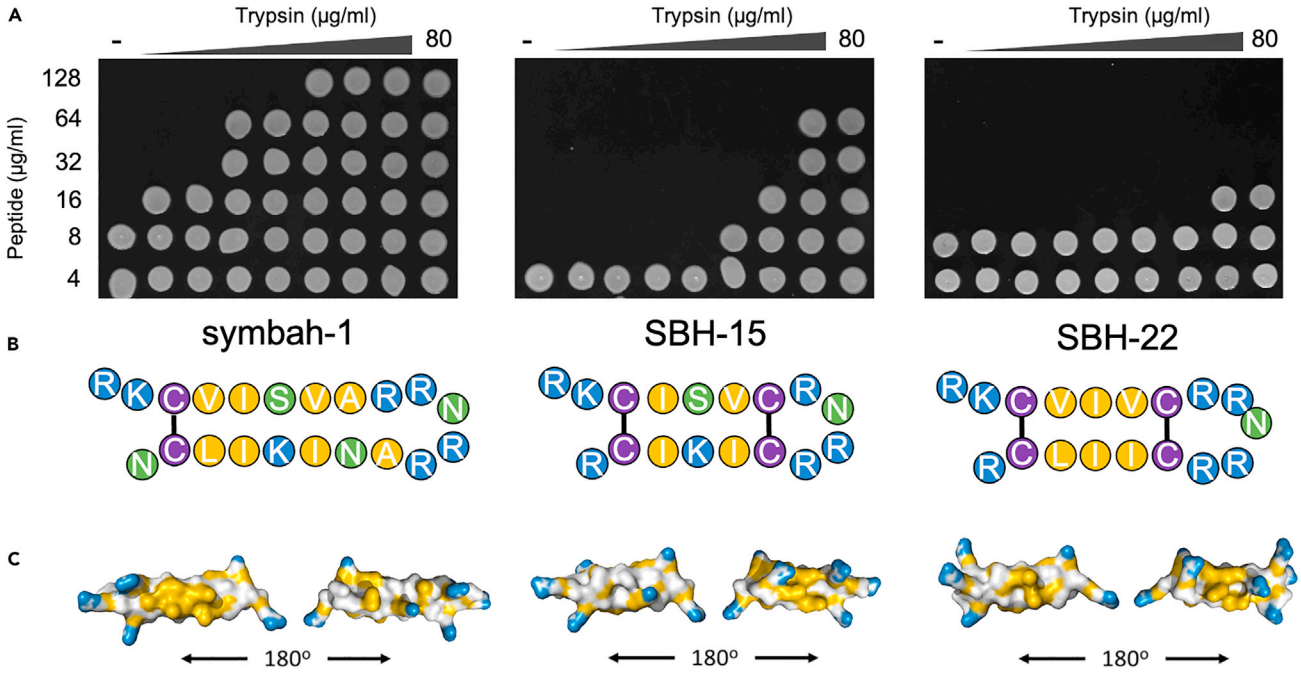

Figure 6. Optimized peptides are more resistant to protease digestion

(A) Representative images of five microliters of overnight culture from MIC assays spotted on LB agar. Columns have 2-fold increasing concentrations of trypsin protease and rows have 2-fold dilutions of peptide.

(B) Model diagrams of symbah-1, SBH-15, and SBH-22 residues in a β-hairpin conformation (blue = charged, yellow = hydrophobic, green = polar, purple = cysteine).

(C) Charge and hydrophobicity surface distributions based on AlphaFold v2 predicted structures (yellow = hydrocarbons with no polar substitutions, blue = nitrogen atoms of lysine and arginine, white = all remaining atoms and polar backbone).

without any increase in hemolysis, making them ideal lead β-AMP candidates for further optimization and therapeutic evaluation similar to what has been done with natural β-AMPs (Edwards et al., 2017; Elliott et al., 2020; Orlov et al., 2019). Higher purity, amidated SBH-15 did not show any additional improvement in its potency (Table 1).

Optimized peptides are more resistant to protease digestion

To help determine whether an increase in serum activity may be due to increased serum protease resistance, trypsin lability was determined for symbah-1, SBH-15, and SBH-22 by measuring their MBC against *A. baumannii* AB5075 with increasing concentrations of trypsin protease in the media. SBH-15 and SBH-22 retained all activity at 16-fold and 64-fold higher trypsin concentrations than symbah-1, respectively, suggesting their increased serum activity may be a result of reduced serum protease lability (Figure 6A). This could stem from a more constrained macrocyclic structure caused by an additional disulfide bond and matched R-group pairs in the antiparallel β-sheet regions (Figure 6B); 91.8% of SBH-22 was determined to contain two disulfide bonds in PBS, whereas only 37.3% of SBH-15 contained two disulfide bonds (Table 1). This could help further explain the difference seen in resistance to trypsin digestion between the two, although we cannot rule out other possibilities such as differences in serum affinity as additional contributing factors. Interestingly, SBH-15 and SBH-22 also contain very different distributions of hydrophobicity and charge in AlphaFold2 modeled tertiary structures (Figure 6C). Together, data presented here could be used to help inform the design of a macrocyclic β-hairpin peptide library. Our findings imply such design should include multiple potential disulfide bonds and theoretically matched R-group pairings in the antiparallel β-sheet regions to promote serum activity and protease resistance.

DISCUSSION

SLAY can rapidly identify synthetic antibiotic peptides in a high-throughput manner. Although they are translated in linear form, our results show SLAY can identify macrocyclic peptides generated through

spontaneous formation of disulfide bridges. Symbah-1 is shown here to have a macrocyclic, β-hairpin structure and broad-spectrum activity against both gram-positive and gram-negative MDR pathogens without readily observed resistance. Interestingly, the MIC of symbah-1 is altered depending on the media used. This was also observed with known antibiotics (Figure 4B). The reason for the differences in MIC between MH and RPMI was not elucidated here but may be due to differences in carbon source, salt, and or buffer concentrations affecting bacterial growth or peptide stability. RPMI was chosen due to differences in host salt and buffer conditions and may help better mimic conditions in the human body.

Our SBH optimization library identified several peptides retaining activity in serum. This is likely due to a more constrained peptide structure resulting in decreased serum protease lability. The addition of a second disulfide bond in SBH peptides was the single most predictive attribute in retention of serum activity, although it was not sufficient for retained activity on its own. SBH-15 and SBH-22, the peptides retaining the greatest serum activity, also contain differing theoretically matched R-groups within the antiparallel β-sheet region of the peptide. SBH-15 has alternating polar/charged hydrophobic pairings, whereas SBH-22 has only hydrophobic pairs. This creates differences in surface charge and hydrophobicity (Figure 6C), although each peptide's true structure would need to be confirmed experimentally. Interestingly, the predicted amino acid pattern seen in SBH-15 was recently observed in a large proteomic analysis of the β-hairpin motif (DuPai et al., 2021). Such motif predictions paired with the inclusion of potential cysteine pairs could be used in the design and screening of macrocyclic β-hairpin peptide libraries using SLAY in the future (Randall et al., 2022).

Symbah-1 permeabilizes the inner and outer membrane of bacterial cells yet demonstrates low hemolysis relative to naturally occurring β-AMPs with membrane activity. The understanding of what characteristics may dictate bacterial membrane selectivity is not well understood, although conformational flexibility, hydrophobicity, and amphipathicity have been suggested (Edwards et al., 2016; Soundrarajan et al., 2019). One possible explanation for the difference in hemolysis observed between the symbah peptides, protegrin-1, and tachyplesin-1 is the presence of polar amino acids (S, N, T, or Q), especially in the loop region of the β-hairpin. Other β-AMPs with low measured hemolysis previously described in the literature (Edwards et al., 2016) also contain polar residues and contain at least one in their loop region (Figure S9. Presence of polar residues correlates with low hemolysis). Although the presence of polar residues decreasing hemolysis is an intriguing hypothesis, additional experimental validation would be necessary to support such a theory.

The need for novel classes of antibiotics to fight MDR infection is clear. Macrocyclic β-hairpin peptides represent a promising group for future antibiotic development due to their inherent stability, potency, and diverse mechanisms of action. Here we report the discovery of a synthetic macrocyclic β-AMP using surface localized antimicrobial display. This provides evidence that targeted SLAY screens with libraries designed around macrocyclic β-hairpin structure could quickly expand this class' sequence information and help us better understand how certain sequence features impact their stability, potency, and toxicity.

Limitations of the study

Here we demonstrate symbah-1 disrupts the outer and inner membrane of bacteria, is active against six different pathogens, and optimized variants with additional disulfide bonds improve serum activity. We, however, do not demonstrate robust physiological performance beyond murine intraperitoneal infection or more deeply characterize symbah peptide's mechanism of action or membrane interactions. This would require further studies examining multiple routes of infection and delivery, peptide pharmacokinetics/pharmacodynamics, toxicology, and biochemical and molecular dynamic modeling studies of peptide-membrane interactions. The breadth and specificity of activity of symbah peptides could also be expanded by measuring activity in a more complete clinical sample of bacterial pathogens in the future.

STAR★METHODS

Detailed methods are provided in the online version of this paper and include the following:

- KEY RESOURCES TABLE
- RESOURCE AVAILABILITY
  - Lead contact
  - Materials availability
  - Data and code availability

SUPPLEMENTAL INFORMATION

Supplemental information can be found online at https://doi.org/10.1016/j.isci.2021.103611.

ACKNOWLEDGMENTS

We would like the thank the University of Texas Mass Spectrometry Facility and the Targeted Therapeutic Drug Discovery and Development Program for access to training and equipment. We would also like to thank Dr. Lindsey Shaw and Dr. George Georgiou for kindly sharing bacterial strains. This work was funded by grants from the National Institutes of Health (AI125337, AI148419, AI159203), the Welch Foundation (F-1870), the Defense Threat Reduction Agency (HDTRA1-17-C0008), and Tito's Handmade Vodka.

AUTHOR CONTRIBUTIONS

The initiation, conceptualization, and methodologies were conceived by JRR, BWD, and SAA. Experimental investigation was performed by JRR, GD, RMF, SAA, and IMR. Bacteriology, including measurement of MIC, MBC, growth, and killing curves were performed by JRR and GD. Propidium iodide uptake was performed by RMF. Circular dichroism was performed by GD and RMF. Mass spec analysis was performed by JRR and IMR. Hemolysis and pull-downs were performed by JRR. Isolation of RNA and RNAseq analysis was performed by SAA and CDD. Visualization of data was performed by JRR and TJC. The original draft was written by JRR with editing help and project supervision from BWD.

DECLARATION OF INTERESTS

The authors have no competing interests to declare.

Received: August 31, 2021
Revised: November 16, 2021
Accepted: December 8, 2021
Published: January 21, 2022

SUPPORTING CITATIONS

The following references appear in the Supplemental Information: Arroyo et al., 2011, Gallagher, 2019.

REFERENCES

Andolina, G., Bencze, L.-C., Zerbe, K., Müller, M., Steinmann, J., Kocherla, H., Mondal, M., Sobek, J., Moehle, K., Malojčić, G., et al. (2018). A peptidomimetic antibiotic interacts with the periplasmic Domain of LptD from Pseudomonas aeruginosa. ACS Chem. Biol. *13*, 666–675. https://doi.org/10.1021/acschembio.7b00822.

Arroyo, L.A., Herrera, C.M., Fernandez, L., Hankins, J.V., Trent, M.S., and Hancock, R.E.W. (2011). The pmrCAB operon mediates polymyxin resistance in acinetobacter baumannii ATCC 17978 and clinical isolates through phosphoethanolamine modification of lipid A. Antimicrob. Agents Chemother. *55*, 3743–3751. https://doi.org/10.1128/AAC.00256-11.

Avitabile, C., D'Andrea, L.D., and Romanelli, A. (2014). Circular Dichroism studies on the interactions of antimicrobial peptides with bacterial cells. Sci. Rep. *4*, 4293. https://doi.org/10.1038/srep04293.

Berman, H.M., Westbrook, J., Feng, Z., Gilliland, G., Bhat, T.N., Weissig, H., Shindyalov, I.N., and

Bourne, P.E. (2000). The protein data bank. Nucleic Acids Res. *28*, 235–242. https://doi.org/10.1093/nar/28.1.235.

Centers for Disease Control and Prevention (U.S.) (2019). Antibiotic Resistance Threats in the United States, 2019 (Centers for Disease Control and Prevention (U.S.)). https://doi.org/10.15620/cdc:82532.

Connolly, M.L. (1983). Analytical molecular surface calculation. J. Appl. Cryst. *16*, 548–558. https://doi.org/10.1107/S0021889883010985.

Dale, G.E., Halabi, A., Petersen-Sylla, M., Wach, A., and Zwingelstein, C. (2018). Pharmacokinetics, tolerability, and safety of murepavadin, a novel antipseudomonal antibiotic, in subjects with mild, moderate, or severe renal function impairment. Antimicrob. Agents Chemother. *62*, e00490. https://doi.org/10.1128/AAC.00490-18.

Delano, W.L. (2002). PyMOL: an open-source molecular graphics tool. Ccp4 Newsl. Pro Crystallogr.

Delmont, T.O., Gaia, M., Hinsinger, D.D., Fremont, P., Guerra, A.F., Eren, A.M., Vanni, C., Kourlaiev, A., d'Agata, L., Clayssen, Q., et al. (2020). Functional repertoire convergence of distantly related eukaryotic plankton lineages revealed by genome-resolved metagenomics. BioRxiv. https://doi.org/10.1101/2020.10.15.341214.

DuPai, C.D., Davies, B.W., and Wilke, C.O. (2021). A systematic analysis of the beta hairpin motif in the Protein Data Bank. Protein Sci. *30*, 613–623. https://doi.org/10.1002/pro.4020.

Edwards, I.A., Elliott, A.G., Kavanagh, A.M., Zuegg, J., Blaskovich, M.A.T., and Cooper, M.A. (2016). Contribution of amphipathicity and hydrophobicity to the antimicrobial activity and cytotoxicity of β-hairpin peptides. ACS Infect. Dis. *2*, 442–450. https://doi.org/10.1021/acsinfecdis.6b00045.

Edwards, I.A., Elliott, A.G., Kavanagh, A.M., Blaskovich, M.A.T., and Cooper, M.A. (2017). Structure-activity and -toxicity relationships of the antimicrobial peptide tachyplesin-1. ACS Infect. Dis. *3*, 917–926. https://doi.org/10.1021/acsinfecdis.7b00123.

Elliott, A.G., Huang, J.X., Neve, S., Zuegg, J., Edwards, I.A., Cain, A.K., Boinett, C.J., Barquist, L., Lundberg, C.V., Steen, J., et al. (2020). An amphipathic peptide with antibiotic activity against multidrug-resistant Gram-negative bacteria. Nat. Commun. *11*, 3184. https://doi.org/10.1038/s41467-020-16950-x.

Fahrner, R.L., Dieckmann, T., Harwig, S.S., Lehrer, R.I., Eisenberg, D., and Feigon, J. (1996). Solution structure of protegrin-1, a broad-spectrum antimicrobial peptide from porcine leukocytes. Chem. Biol. *3*, 543–550. https://doi.org/10.1016/s1074-5521(96)90145-3.

Fehlbaum, P., Bulet, P., Chernysh, S., Briand, J.P., Roussel, J.P., Letellier, L., Hetru, C., and Hoffmann, J.A. (1996). Structure-activity analysis of thanatin, a 21-residue inducible insect defense peptide with sequence homology to frog skin antimicrobial peptides. Proc. Natl. Acad. Sci. U S A *93*, 1221–1225. https://doi.org/10.1073/pnas.93.3.1221.

Gallagher, L.A. (2019). Methods for tn-seq analysis in acinetobacter baumannii. Methods Mol. Biol. *1946*, 115–134. https://doi.org/10.1007/978-1-4939-9118-1_12.

Gentilucci, L., De Marco, R., and Cerisoli, L. (2010). Chemical modifications designed to improve peptide stability: incorporation of non-natural amino acids, pseudo-peptide bonds, and cyclization. Curr. Pharm. Des. *16*, 3185–3203. https://doi.org/10.2174/138161210793292555.

Greenfield, N., and Fasman, G.D. (1969). Computed circular dichroism spectra for the evaluation of protein conformation. Biochemistry *8*, 4108–4116. https://doi.org/10.1021/bi00838a031.

Hagemans, D., van Belzen, I.A.E.M., Morán Luengo, T., and Rüdiger, S.G.D. (2015). A script to highlight hydrophobicity and charge on protein surfaces. Front. Mol. Biosci. *2*, 56. https://doi.org/10.3389/fmolb.2015.00056.

Imai, Y., Meyer, K.J., Iinishi, A., Favre-Godal, Q., Green, R., Manuse, S., Caboni, M., Mori, M., Niles, S., Ghiglieri, M., et al. (2019). A new antibiotic selectively kills Gram-negative pathogens. Nature *576*, 459–464. https://doi.org/10.1038/s41586-019-1791-1.

Jumper, J., Evans, R., Pritzel, A., Green, T., Figurnov, M., Ronneberger, O., Tunyasuvunakool, K., Bates, R., Žídek, A., Potapenko, A., et al. (2021). Highly accurate protein structure prediction with AlphaFold. Nature. https://doi.org/10.1038/s41586-021-03819-2.

Kaur, H., Jakob, R.P., Marzinek, J.K., Green, R., Imai, Y., Bolla, J.R., Agustoni, E., Robinson, C.V., Bond, P.J., Lewis, K., et al. (2021). The antibiotic darobactin mimics a β-strand to inhibit outer membrane insertase. Nature *593*, 125–129. https://doi.org/10.1038/s41586-021-03455-w.

Kokryakov, V.N., Harwig, S.S., Panyutich, E.A., Shevchenko, A.A., Aleshina, G.M., Shamova, O.V., Korneva, H.A., and Lehrer, R.I. (1993). Protegrins: leukocyte antimicrobial peptides that combine features of corticostatic defensins and tachyplesins. FEBS Lett. *327*, 231–236. https://doi.org/10.1016/0014-5793(93)80175-t.

Kushibiki, T., Kamiya, M., Aizawa, T., Kumaki, Y., Kikukawa, T., Mizuguchi, M., Demura, M., Kawabata, S., and Kawano, K. (2014). Interaction between tachyplesin I, an antimicrobial peptide derived from horseshoe crab, and lipopolysaccharide. Biochim. Biophys. Acta *1844*, 527–534. https://doi.org/10.1016/j.bbapap.2013.12.017.

Lam, K.L.H., Ishitsuka, Y., Cheng, Y., Chien, K., Waring, A.J., Lehrer, R.I., and Lee, K.Y.C. (2006). Mechanism of supported membrane disruption by antimicrobial peptide protegrin-1. J. Phys. Chem. B *110*, 21282–21286. https://doi.org/10.1021/jp0630065.

Levy Karin, E., Mirdita, M., and Söding, J. (2020). MetaEuk-sensitive, high-throughput gene discovery, and annotation for large-scale eukaryotic metagenomics. Microbiome *8*, 48. https://doi.org/10.1186/s40168-020-00808-x.

Ling, L.L., Schneider, T., Peoples, A.J., Spoering, A.L., Engels, I., Conlon, B.P., Mueller, A., Schäberle, T.F., Hughes, D.E., Epstein, S., et al. (2015). A new antibiotic kills pathogens without detectable resistance. Nature *517*, 455–459. https://doi.org/10.1038/nature14098.

Luther, A., Bisang, C., and Obrecht, D. (2018). Advances in macrocyclic peptide-based antibiotics. Bioorg. Med. Chem. *26*, 2850–2858. https://doi.org/10.1016/j.bmc.2017.08.006.

Mariani, V., Biasini, M., Barbato, A., and Schwede, T. (2013). lDDT: a local superposition-free score for comparing protein structures and models using distance difference tests. Bioinformatics *29*, 2722–2728. https://doi.org/10.1093/bioinformatics/btt473.

Martin-Loeches, I., Dale, G.E., and Torres, A. (2018). Murepavadin: a new antibiotic class in the pipeline. Expert Rev. Anti Infect. Ther. *16*, 259–268. https://doi.org/10.1080/14787210.2018.1441024.

Mirdita, M., von den Driesch, L., Galiez, C., Martin, M.J., Söding, J., and Steinegger, M. (2017). Uniclust databases of clustered and deeply annotated protein sequences and alignments. Nucleic Acids Res. *45*, D170–D176. https://doi.org/10.1093/nar/gkw1081.

Mirdita, M., Steinegger, M., and Söding, J. (2019). MMseqs2 desktop and local web server app for fast, interactive sequence searches. Bioinformatics *35*, 2856–2858. https://doi.org/10.1093/bioinformatics/bty1057.

Mitchell, A.L., Almeida, A., Beracochea, M., Boland, M., Burgin, J., Cochrane, G., Crusoe, M.R., Kale, V., Potter, S.C., Richardson, L.J., et al. (2020). MGnify: the microbiome analysis resource in 2020. Nucleic Acids Res. *48*, D570–D578. https://doi.org/10.1093/nar/gkz1035.

Moiola, M., Memeo, M.G., and Quadrelli, P. (2019). Stapled peptides-A useful improvement for peptide-based drugs. Molecules *24*, E3654. https://doi.org/10.3390/molecules24203654.

Moura, E.C.C.M., Baeta, T., Romanelli, A., Laguri, C., Martorana, A.M., Erba, E., Simorre, J.-P., Sperandeo, P., and Polissi, A. (2020). Thanatin impairs lipopolysaccharide transport complex assembly by targeting LptC-LptA interaction and decreasing LptA stability. Front. Microbiol. *11*, 909. https://doi.org/10.3389/fmicb.2020.00909.

Mourtada, R., Herce, H.D., Yin, D.J., Moroco, J.A., Wales, T.E., Engen, J.R., and Walensky, L.D. (2019). Design of stapled antimicrobial peptides that are stable, nontoxic and kill antibiotic-resistant bacteria in mice. Nat. Biotechnol. *37*, 1186–1197. https://doi.org/10.1038/s41587-019-0222-z.

Nakamura, T., Furunaka, H., Miyata, T., Tokunaga, F., Muta, T., Iwanaga, S., Niwa, M., Takao, T., and Shimonishi, Y. (1988). Tachyplesin, a class of antimicrobial peptide from the hemocytes of the horseshoe crab (Tachypleus tridentatus). Isolation and chemical structure. J. Biol. Chem. *263*, 16709–16713.

Orlov, D.S., Shamova, O.V., Eliseev, I.E., Zharkova, M.S., Chakchir, O.B., Antcheva, N., Zachariev, S., Panteleev, P.V., Kokryakov, V.N., Ovchinnikova, T.V., et al. (2019). Redesigning arenicin-1, an antimicrobial peptide from the marine polychaeta arenicola marina, by strand rearrangement or Branching, substitution of specific residues, and backbone linearization or

cyclization. Mar. Drugs *17*, E376. https://doi.org/10.3390/md17060376.

Ovchinnikov, S., Mirdita, M., and Steinegger, M. (2021). ColabFold - Making Protein Folding Accessible to All via Google Colab (Zenodo). https://doi.org/10.5281/zenodo.5123297.

Panteleev, P.V., Bolosov, I.A., Balandin, S.V., and Ovchinnikova, T.V. (2015). Structure and biological functions of β-hairpin antimicrobial peptides. Acta Naturae *7*, 37–47. https://doi.org/10.1021/bp9900108.

Panteleev, P.V., Balandin, S.V., Ivanov, V.T., and Ovchinnikova, T.V. (2017). A therapeutic potential of animal β-hairpin antimicrobial peptides. Curr. Med. Chem. *24*, 1724–1746. https://doi.org/10.2174/0929867324666170424124416.

Park, S.J., Georgiou, G., and Lee, S.Y. (1999). Secretory production of recombinant protein by a high cell density culture of a protease negative mutant Escherichia coli strain. Biotechnol. Prog. *15*, 164–167. https://doi.org/10.1021/bp9900108.

Passioura, T. (2020). The road ahead for the development of macrocyclic peptide ligands. Biochemistry *59*, 139–145. https://doi.org/10.1021/acs.biochem.9b00802.

Randall, J.R., and Davies, B.W. (2021). Mining for novel antibiotics. Curr. Opin. Microbiol. *63*, 66–69. https://doi.org/10.1016/j.mib.2021.06.001.

Randall, J.R., DuPai, C.D., and Davies, B.W. (2022). Discovery of antimicrobial peptide macrocycles through bacterial display. Methods Mol. Biol. *2371*, 287–298. https://doi.org/10.1007/978-1-0716-1689-5_15.

Sehnal, D., Bittrich, S., Deshpande, M., Svobodová, R., Berka, K., Bazgier, V., Velankar, S., Burley, S.K., Koča, J., and Rose, A.S. (2021). Mol* Viewer: modern web app for 3D visualization and analysis of large biomolecular structures. Nucleic Acids Res. *49*, W431–W437. https://doi.org/10.1093/nar/gkab314.

Shrivastava, S.R., Shrivastava, P.S., and Ramasamy, J. (2018). Responding to the challenge of antibiotic resistance: world Health organization. J. Res. Med. Sci. *23*, 21. https://doi.org/10.4103/1735-1995.228593.

Sievers, F., Wilm, A., Dineen, D., Gibson, T.J., Karplus, K., Li, W., Lopez, R., McWilliam, H., Remmert, M., Söding, J., et al. (2011). Fast, scalable generation of high-quality protein multiple sequence alignments using Clustal Omega. Mol. Syst. Biol. *7*, 539. https://doi.org/10.1038/msb.2011.75.

Silver, L.L. (2011). Challenges of antibacterial discovery. Clin. Microbiol. Rev. *24*, 71–109. https://doi.org/10.1128/CMR.00030-10.

Soundrarajan, N., Park, S., Le Van Chanh, Q., Cho, H.-S., Raghunathan, G., Ahn, B., Song, H., Kim, J.-H., and Park, C. (2019). Protegrin-1 cytotoxicity towards mammalian cells positively correlates with the magnitude of conformational changes of the unfolded form upon cell interaction. Sci. Rep. *9*, 11569. https://doi.org/10.1038/s41598-019-47955-2.

Steinegger, M., and Söding, J. (2018). Clustering huge protein sequence sets in linear time. Nat. Commun. *9*, 2542. https://doi.org/10.1038/s41467-018-04964-5.

Tucker, A.T., Leonard, S.P., DuBois, C.D., Knauf, G.A., Cunningham, A.L., Wilke, C.O., Trent, M.S., and Davies, B.W. (2018). Discovery of next-generation antimicrobials through bacterial self-screening of surface-displayed peptide libraries. Cell *172*, 618–628.e13. https://doi.org/10.1016/j.cell.2017.12.009.

Vetterli, S.U., Zerbe, K., Müller, M., Urfer, M., Mondal, M., Wang, S.-Y., Moehle, K., Zerbe, O., Vitale, A., Pessi, G., et al. (2018). Thanatin targets the intermembrane protein complex required for lipopolysaccharide transport in Escherichia coli. Sci. Adv. *4*, eaau2634. https://doi.org/10.1126/sciadv.aau2634.

Zipperer, A., Konnerth, M.C., Laux, C., Berscheid, A., Janek, D., Weidenmaier, C., Burian, M., Schilling, N.A., Slavetinsky, C., Marschal, M., et al. (2016). Human commensals producing a novel antibiotic impair pathogen colonization. Nature *535*, 511–516. https://doi.org/10.1038/nature18634.

Zong, Y., Fang, F., Meyer, K.J., Wang, L., Ni, Z., Gao, H., Lewis, K., Zhang, J., and Rao, Y. (2019). Gram-scale total synthesis of teixobactin promoting binding mode study and discovery of more potent antibiotics. Nat. Commun. *10*, 3268. https://doi.org/10.1038/s41467-019-11211-y.

Zorzi, A., Deyle, K., and Heinis, C. (2017). Cyclic peptide therapeutics: past, present and future. Curr. Opin. Chem. Biol. *38*, 24–29. https://doi.org/10.1016/j.cbpa.2017.02.006.

STAR★METHODS

KEY RESOURCES TABLE

REAGENT or RESOURCE	SOURCE	IDENTIFIER
Biological samples		
Single donor human red blood cells	Innovative Research	IWB3ALS
Chemicals, peptides, and recombinant proteins		
Carbenicillin	Goldbio	C-103-100
Tetracycline	Goldbio	T-101-25
RPMI 1640	ATCC	30–2001
Mueller-hinton broth	BD	275730
LB broth with agar	Sigma-Aldrich	L3147-1KG
10× PBS	Fisher Scientific	BP399-4
Cyclophosphamide monohydrate	MP Biomedicals	0215074910
Propidium iodide	Sigma-Aldrich	81845-25MG
Triton X-100	Fisher Scientific	9002-93-1
Direct-zol	Genesee	11-330T
EcoRI-HF	New England Biolabs	R3101S
SalI-HF	New England Biolabs	R3138L
Dithiothreitol	Goldbio	DTT50
IPTG	Goldbio	I2481C50
Lipopolysaccharides from E. coli 026:B6	Sigma	CAT#L8274
T4 ligase	New England Biolabs	M0202L
TURBO DNA-free kit	Invitrogen	AM1907
Deposited data		
RNA sequencing	This paper	SRA: PRJNA749374
Experimental models: Organisms/strains		
Female Domestic CD1 mice	Charles River	
Software and algorithms		
Prism 9	GraphPad	
PyMol v2.5	(49)	
Clustal Omega	(57)	
AlphaFold V2	(29)	
MMseqs2	(41)	
Mol* 3D viewer	(54, 55)	
Other		
Polypropylene 96 well plates	Corning	3879
Flat bottom 96 well plates	Genesee	25-104
Black walled clear bottom 96-well plate	Falcon	353219
2 mL autosampler vials	Fisherbrand	03-391-8
Autosampler vial small volume inserts	Restek	21776
Petri dishes, stackable	GenClone	32-106
0.1 cm path-length quartz cuvette	Jasco	J/1103-1072
1 mm diameter zirconia/silica beads	BioSpec	11079110z

RESOURCE AVAILABILITY

Lead contact

Further information and requests for resources and reagents should be directed to and will be fulfilled by the lead contact, Bryan Davies (bwdavies@austin.utexas.edu).

Materials availability

Tables containing all bacterial strains (Table S4. Bacterial strains used), peptides (Table S5. Peptides used), plasmids (Table S6. Plasmids used), and oligonucleotides (Table S7. Oligonucleotides used) in this work can be found in the supplementary information. All chemicals, biologics, model organisms and software used are listed in the key resources table.

Data and code availability

RNA-seq data have been deposited in the SRA database and are publicly available as of the date of publication. The accession number is listed in the key resources table. Any additional information required to reanalyze the data reported in this paper is available from the lead contact upon request.

METHOD DETAILS

Peptide synthesis

All peptides used in this work were synthesized commercially by GenScript's custom peptide synthesis service. Each peptide goes through reverse phase high performance liquid chromatography (RP-HPLC) and mass spectrometry quality control analysis to confirm purity and molecular weight. Lyophilized peptides were resuspended in water at 10 mg/mL and then adjusted to a 5 mg/mL stock in water based on A_{205} extinction coefficient. A full list of all of the peptides used and their purity can be found in Table S4.

Peptide display growth inhibition

Overnight cultures of *E. coli* W3110 containing either pMMBEH67_lpp-ompA-2xNR-2xHA or pMMBEH67_lpp-ompA-2xNR-symbah-1 were diluted to an OD_{600} of 0.01 in 5 mL cultures of LB supplemented with 75 μg/mL carbenicillin. Each culture was grown to an OD_{600} = 0.7 at 37°C and then back diluted to an OD_{600} = 0.01. 200 ul of culture were added to wells of a 96 well plate in triplicate with or without 1 mM IPTG. The plate was then grown shaking at 37°C and the OD_{600} measured every 15 minutes for 3 hours using a SpectraMax Plus plate reader. Error bars represent one standard deviation between triplicate samples.

Minimum inhibitory concentration

Stock peptides were diluted to 256 μg/mL in 350 μLs of either MH or RPMI media and 100 μL was aliquoted in the top row of a polypropylene 96 well plate in triplicate. Peptides were then serial diluted 2-fold down columns of the plate by taking 50 μL from each well and mixing with 50 mL of media in the well below. Separately, each bacterial strain was grown overnight in 5 mL MH media at 37°C. Cells from these cultures were diluted to a concentration of 1×10^6 cells/mL in either MH or RPMI and 50 μL were added to each well of the 96 well plate containing diluted peptide resulting in wells with a final cell concentration of 5×10^5 cell/mL. Human serum and trypsin were added to the diluted cells at twice the reported concentration where described. Plates were wrapped twice in parafilm and incubated at 37°C for 18–24 h. Wells were examined by eye against wells with no bacteria for signs of growth. MICs were reported as the minimum concentration with no observable growth. In cases were triplicate samples differed, the concentration supported by the median of the three replicates was reported.

Minimum bactericidal concentrations

MBCs were determined by removing 5 μL of culture from each well of the polypropylene 96 well plate from an overnight MIC assay and plating on large LB agar filled petri dishes. These dishes were incubated an additional 18 h at 37°C and the lowest antibiotic concentration where zero growth was observed was called as the MBC. In cases were triplicate samples differed, the concentration supported by the median of the three replicates was reported.

Killing curve

Experimental set up was the same as described for the MIC method in 96 well plates above but 10 ul samples were taken from each well at the indicated time points, serial diluted 10-fold, and immediately plated on a large LB agar filled Petri dish. After overnight incubation at 37°C, CFUs were counted and reported as an average of triplicate samples with error bars representing one standard deviation.

Circular dichroism

Stock peptides were diluted in 10 mM potassium phosphate pH 7.4 to a volume of 200 ul. LPS was added to samples at the reported concentrations where appropriate. Samples were incubated for two hours at room temperature and then analyzed using a Jasco-815 CD spectrometer with a 0.1 cm path-length quartz cuvette at the Targeted Therapeutic Drug Discovery & Development Program Core at UT Austin. The CD spectra were collected using far-UV spectra (190–260 nm) with background corrected for either sodium phosphate buffer alone or the buffer with corresponding amounts of LPS. Reported spectra are an average of three separate spectra obtained from the same sample.

High resolution mass spectrometry

Stock peptides were diluted into the stated media (MH ± 10 mM DTT, PBS) at 0.1 mg/mL in a volume of 100 ul and placed into 2 mL autosampler vials with small volume inserts. Samples were separated by an C8 liquid chromatography column and an Extracted Ion Chromatogram (EIC) was extracted for the +5 charge state peaks. Mass spectra were generated for each LC peak using an Agilent Technologies 6546 Accurate-Mass Q-TOF LC/MS instrument. Analysis was performed using Agilent MassHunter Qualitative software v10. The +5 charge state isotope distribution was for each LC peak from each sample was compared to predicted distributions created using Agilent's Isotope Distribution Calculator. Percentages of molecules with disulfide bonds was determined by comparing the area under the curve for each LC peak over the total area of all peaks.

Intraperitoneal infection

Female CD1 mice were used for this assay. A dose of 150 mg/kg of cyclophosphamide, comprised of 70% 1× PBS and 30% PEG, was administered 4 days before bacterial inoculation in a total volume of 0.15 mL intraperitoneal injection per mouse. A second dose of 100 mg/kg cyclophosphamide was administered 1 day before bacterial inoculation with the same injection volume and method. *A. baumannii* AB5075 was grown in LB media to log phase of growth and pelleted then resuspended in RPMI media to 1×10^8 cells/mL. In the negative control and symbah-1 treatment groups, 0.1 mL of RPMI or RPMI with bacteria at a dose of 1×10^7 CFUs per dose was intraperitoneally administered. 15 min after the initial bacterial inoculation, symbah-1 was intraperitoneally administered at a loading dose of 5 mg/kg in 0.1 mL RPMI media. The negative control group did not receive any treatment. Six hours after bacterial inoculation, the liver and kidneys of euthanized mice were removed, homogenized with the BioSpec BeadBeater, serial diluted and evaluated by plating 10-fold dilutions on an LB agar supplemented with 75 μg/mL carbenicillin. Significance was determined using an unpaired two-tailed t test (*$P < 0.05$).

Propidium iodide uptake

E. coli W3110 was grown overnight in lysogeny broth (LB) at 37°C with shaking at 225 rpm. Cultures were synchronized to exponential phase, washed two times with phosphate buffered saline (PBS) and standardized to an OD 600 of 0.1 in PBS supplemented with 50 mM Glucose. Propidium iodide was added to the culture at 10 μg/mL (15 μM) and 50 μL of culture was added to a black walled, clear bottom 96-well plate containing 50 μL of the peptide serial diluted from 64 to 1 μg/mL using 2-fold dilutions. The fluorescence was read after 15 min using excitation of 490 nm and emission of 617 nm. Background fluorescence from samples with no peptide were subtracted from values shown. Error bars represent the standard deviation between triplicate samples (n = 3).

Hemolysis

Single donor human red blood cells were washed in PBS and adjusted to a concentration of $1x10^9$ blood cells/mL. 197.44 uL were placed into each well of a polypropylene 96 well plate. 2.56 μL of each 5 mg/mL stock peptide were added to triplicate wells to final concentration 128 μg/mL. Water was used as a negative control and a final concentration of 1% Triton X-100 as a positive control. Plates were incubated for 3 h at 37°C. Following incubation samples were centrifuged at 4000 RPM for 20 min and 100 ul of supernatant was

transferred to a flat bottom 96 well plate. Percent hemolysis for each sample was determined by normalizing the absorbance at 540 nm for each sample to the average negative control and dividing by the average 540 absorbance for 1% Triton X-100 (100% hemolysis). Error bars represent one standard deviation of triplicate samples.

Symbah peptide tertiary structure predictions and modeling

Three dimensional structures for symbah-1 and all its variants were predicted using AlphaFold v2 (Jumper et al., 2021). MMseqs2 (Mirdita et al., 2019) was used to search the peptide sequences against UniRef (Mirdita et al., 2017) and large environmentally sourced protein sequence databases BFD (Steinegger and Söding, 2018), Mgnify (Mitchell et al., 2020), MetaEuk (Levy Karin et al., 2020), and SMAG (Delmont et al., 2020) all clustered by sequences having at least 30% sequence identity. Hits from MMSeqs2 were used to generate multiple sequence alignments, which were used along with the AlphaFold pipeline to extract features. These features were provided to the AlphaFold algorithm via the ColabFold pipeline to predict five three dimensional structures for each peptide (Ovchinnikov et al., 2021). For each predicted structure, the predicted alignment error was calculated, and the structure was assessed using the Local Distance Difference Test for each residue (Mariani et al., 2013).

The top structural predictions for SBH peptides were visualized using PyMol v2.5 (Delano, 2002) to show the presence of anti-parallel β-sheets and disulfide bonds. Additionally, the molecular surface of the predicted structures of symbah-1, SBH-15, and SBH-22 were visualized calculating the solvent excluded surface (Connolly, 1983), and colored using the YRB scheme to visualize amphipathic faces (Hagemans et al., 2015).

Natural β-hairpin antimicrobial peptide structures

Tertiary rainbow ribbon models of the protegrin-1 and tachyplesin-1 structures (Fahrner et al., 1996; Kushibiki, et al., 2014), and symbah-1 AlphaFold v2 model were visualized using Mol* 3D viewer (Berman et al., 2000; Sehnal et al., 2021).

Plasmid cloning. pMMBEH67_lpp_ompA_2×(NR)T_symbah-1 was cloned by amplifying the 2×(NR)Tether gBlock using primers oJR572 and oJR557. The resulting PCR product and the pMMBEH67_lpp_ompA plasmid were digested with KpnI and SalI, ligated with T4 ligase and transformed into *E. coli* W3110 competent cells via electroporation and plated on LB agar supplemented with 75 ug/mL carbenicillin.

Plasmids for AB5075 gene overexpression were cloned by digesting gblocks with the corresponding coding region for each gene and added restriction sites (EcoRI and SalI) and pMMBEH67 Tet^R with EcoRI and SalI and ligating with T4 ligase. Plasmids were transformed into electrocompetent *A. baumannii* AB5075 cells and plated on LB supplemented with 10 μg/mL tetracycline.

RNA sequencing

A. baumannii Ab5075 from overnight culture was back diluted and grown to mid-log phase (OD600 = 0.3–0.5) at 37°C. Six 3 mL samples were then normalized to OD = 0.3; three were treated with amidated symbah-1 in water at 8 ug/mL, and the remaining three were treated with water as a control. The samples were incubated for 60 min. Two ml of bacteria culture were pelleted by centrifugation at 3,500 g for 10 min at room temperature. The Direct-zol protocol was then applied to extract total RNAs from the cell pellets. To ensure that the DNA was completely removed, DNase digestion was performed. Sequencing was performed by the UT Austin GSAF core. Reads were trimmed of adapter sequences using flexbar (https://pubmed.ncbi.nlm.nih.gov/28541403/) and then assessed for quality via FastQC (https://www.bioinformatics.babraham.ac.uk/projects/fastqc/). Next, trimmed reads were mapped to a transcriptome derived from assembly ASM96381 (https://www.ncbi.nlm.nih.gov/assembly/GCA_000963815.1) using Kallisto (https://www.nature.com/articles/nbt.3519). Finally, log2fold change estimates and other relevant statistics were calculated using DESeq2 (https://genomebiology.biomedcentral.com/articles/10.1186/s13059-014-0550-8).

His-symbah-1 pull down

A. baumannii 17,978 was grown in MH broth overnight, back diluted 1:100 in fresh MH and grown to mid-log phase (OD600 = 0.3–0.5) at 37°C. Cells were split into two 1 mL cultures and challenged with either 64 mg/mL symbah-1 or 6xHis tagged symbah-1 and allowed to grow at 37°C for thirty minutes. Cultures were then lysed using sonication and 50 μL of Ni^{2+} agarose bead slurry in PBS was added to each lysed

sample and left rotating at 4°C for 30 min. The beads were pelleted in a centrifuge at 4000 rpm for 5 min and the supernatant removed and the pellet washed with 1 mL of PBS three times. 50 μL of PBS with 500 mM IPTG was then added to the culture to eluted bound proteins and the supernatant run into an SDS-PAGE gel, excised, and submitted for MALDI-TOFF MS analysis through the UT Austin Proteomics core to identify the presence score and p values of any *A. baumannii* 17,978 proteins detected.

Beta-AMP alignment

The sequences of all the beta-AMPs listed were aligned via Clustal Omega software (Sievers et al., 2011) (https://www.ebi.ac.uk/Tools/msa/clustalo/). GRAVY scores were calculated using Expasy ProtParam tool (https://web.expasy.org/protparam/)

QUANTIFICATION AND STATISTICAL ANALYSIS

For peptide growth inhibition, peptide kill curves, PI uptake, and hemolysis the mean +/− one standard deviation of triplicate reactions (n = 3) was calculated and represented with error bars in graphs and a ± in tables. For MICs and MBCs triplicate samples (n = 3) were tested and each plotted as dots with the median represented as bars in graphs. This median is also reported in tables. Statistical significance for murine intraperitoneal infections was determined by an unpaired two-tailed t test (*P < 0.05) using Prism software (n ≥ 4). For RNAseq analysis sequencing reads were trimmed of adapter sequences using flexbar (https://pubmed.ncbi.nlm.nih.gov/28541403/) and then assessed for quality via FastQC (https://www.bioinformatics.babraham.ac.uk/projects/fastqc/). Next, trimmed reads were mapped to a transcriptome derived from assembly ASM96381 (https://www.ncbi.nlm.nih.gov/assembly/GCA_000963815.1) using Kallisto (https://www.nature.com/articles/nbt.3519). Finally, log2fold change estimates and other relevant statistics were calculated using DESeq2 (https://genomebiology.biomedcentral.com/articles/10.1186/s13059-014-0550-8).